PLOS ONE

Peroxidase-Like Catalytic Activity of Ag$_3$PO$_4$ Nanocrystals Prepared by a Colloidal Route

Yuanjun Liu[1], Guoxing Zhu[2,3]*, Jing Yang[2], Aihua Yuan[1]*, Xiaoping Shen[2]

1 School of Environmental and Chemical Engineering, Jiangsu University of Science and Technology, Zhenjiang, China, 2 School of Chemistry and Chemical Engineering, Jiangsu University, Zhenjiang, China, 3 State Key Laboratory of Coordination Chemistry, Nanjing University, Nanjing, P. R. China

Abstract

Nearly monodispersed Ag$_3$PO$_4$ nanocrystals with size of 10 nm were prepared through a colloidal chemical route. It was proven that the synthesized Ag$_3$PO$_4$ nanoparticles have intrinsic peroxidase-like catalytic activity. They can quickly catalyze oxidation of the peroxidase substrate 3, 3, 5, 5-tetramethylbenzidine (TMB) in the presence of H$_2$O$_2$, producing a blue color. The catalysis reaction follows Michaelis-Menten kinetics. The calculated kinetic parameters indicate a high catalytic activity and the strong affinity of Ag$_3$PO$_4$ nanocrystals to the substrate (TMB). These results suggest the potential applications of Ag$_3$PO$_4$ nanocrystals in fields such as biotechnology, environmental chemistry, and medicine.

Data Availability: The authors confirm that all data underlying the findings are fully available without restriction. All relevant data are within the paper.

Competing Interests: The authors have declared that no competing interests exist.

* Email: zhuguoxing@ujs.edu.cn (GZ); aihuayuan@just.edu.cn (AY)

Introduction

Owing to its excellent photocatalytic properties and broad range of applications such as in water-splitting, photocatalytic reactions, silver phosphate has got extensive study and has become a well studied material [1]. Especially, partly owing to the highly dispersive Ag s-Ag s bands without localized d states [2], Ag$_3$PO$_4$ semiconductor exhibits extremely high photooxidative ability for O$_2$ evolution from water as well as organic dye decomposition under visible light irradiation [3–6]. A much higher quantum efficiency (up to 90%) than the previously reported values at wavelengths longer than 420 nm was also achieved with it [1].

Up to now, various methods have been proposed to further enhance and optimize the photoelectric and photocatalytic properties of Ag$_3$PO$_4$ via microstructure control or forming composites with other components to improve its stability, bandgap structure and surface area [7–12]. Although extensive studies have been made for the photocatalytic applications of various Ag$_3$PO$_4$ micro-/nanoparticles and their composites, the application of Ag$_3$PO$_4$ in biological systems, for example used as biocatalyst, has rarely been studied, while the presence of phosphorus in biological systems is well known.

Recently, it was found that Fe$_3$O$_4$ nanoparticles have intrinsic enzyme-like activity similar to peroxidases found in nature, though Fe$_3$O$_4$ are usually thought to be biological and chemical inert [13]. After that, several kinds of micro/nanoparticles with smaller size or special structure were prepared for developing enzyme mimics, including the ferromagnetic nanoparticles with peroxidase-like activity [14–23], ceria oxide nanoparticles [24–27], and V$_2$O$_5$ nanowires [28], carbon-based nanomaterials [29–36] and so on [37–42]. In contrast to natural enzymes, nanoparticles-based enzyme mimics own prominent advantages. First, they have greater resistance to extremes of pH and temperature, while natural enzymes are usually sensitive to the external conditions and also easily lose their activity. Secondly, nanoparticles-based mimic enzymes have higher stability, while natural enzymes can be digested by proteases. Thirdly, with the extensive development of nanoscience and nanotechnology in the past three decades, the preparation and surface modification of various nanoobjects can be easily carried out, while the synthesis and purification of natural enzymes are still time-consuming, expensive, and also difficult [14].

Exploitation of new functions of known nanomaterials is one of the most attractive aspects in nanoscience [37]. Inspired by the above pioneering research, we investigated the peroxidase-like activity of Ag$_3$PO$_4$ nanocrystals, considering that some Ag-based metal alloy nanoparticles own intrinsic peroxidase-like activity. Ag$_3$PO$_4$ nanoparticles with smaller size were obtained via a simple colloidal route. It was found that the obtained Ag$_3$PO$_4$ nanoparticles show their ability to catalyze peroxidatic reactions in aqueous media. The kinetic parameters were also tested and compared. The reaction catalyzed by these Ag$_3$PO$_4$ nanoparticles followed a Michaelis-Menten kinetic behavior with an excellent catalytic activity, making it a promising mimic of peroxidase. The new application of Ag$_3$PO$_4$ as peroxidase mimic will add new content to this interesting material.

Results and Discussion

A colloidal route was employed for the preparation of Ag$_3$PO$_4$ nanoparticles because it can produce Ag$_3$PO$_4$ nanoparticles with smaller size [6]. The preparation was carried out at room

temperature with H$_3$PO$_4$ and AgNO$_3$ as raw materials, while toluene and oleylamine were used as solvent and surfactant. The crystal phase of the obtained Ag$_3$PO$_4$ nanoparticles was first determined by X-ray diffraction (XRD). Fig. 1a shows the corresponding XRD pattern, which can be easily indexed to cubic Ag$_3$PO$_4$ with JCPDS No. 06-0505. The relatively strong peaks at 21.3, 30.1, 33.6, 36.9, 53.1, 55.3, and 57.6° corresponds to the (110), (200), (210), (211), (222), (320), and (321) crystal planes of cubic Ag$_3$PO$_4$, respectively. No diffraction peak from Ag with zero-valent state is observed in the pattern. This reveals pure Ag$_3$PO$_4$ is obtained with this simple route. It should be noted that the XRD pattern shows relatively broad peak, indicating the smaller size of Ag$_3$PO$_4$ nanocrystals according to Scherrer formula. Fig. 1b shows a typical transmission electron microscopy (TEM) image of the obtained Ag$_3$PO$_4$ nanocrystals, from which spherical particles with small size are observed. The Ag$_3$PO$_4$ particles show relatively uniform size. The average diameter is about 10 nm.
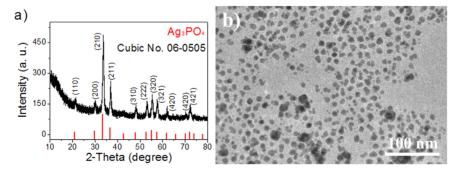
Before property investigation, the obtained Ag$_3$PO$_4$ nanocrystals were firstly treated through usual ligand exchange route to transfer it to being hydrophilic state. Peroxidase-like activity of the Ag$_3$PO$_4$ nanocrystals was evaluated in the catalysis oxidation of a commonly used peroxidase substrate, 3, 3′, 5, 5′-tetramethylbenzidine sulfate (TMB), in the presence of H$_2$O$_2$. TMB is colorless and can be oxidized slowly by H$_2$O$_2$ (Fig. 2). The often observed oxidation products are two colored products [43]. The first product is a blue charge-transfer complex of diamine, which are formed in rapid equilibrium with the radical cation. Its maximal absorption wavelength locates at ~370 and ~652 nm. Another product is a yellow diimine, which is generated by further oxidation of the diamine with excess H$_2$O$_2$ or strong acidic condition. The diimine product is stable in acidic conditions with maximal absorption wavelength of 450 nm. The first-step reaction with the formation of blue diamine is often used as a model process to evaluate activity of peroxidases.

As can be seen in Figure 3, our preliminary experiment shows that Ag$_3$PO$_4$ nanocrystals can catalyze the oxidation of TMB by H$_2$O$_2$ in NaAc buffer producing a blue solution (inset of Figure 3), suggesting the formation of charge-transfer complex of diamine. The typical absorbance peak of this oxidation product of TMB is at 652 nm. The reaction system will turn to be yellow if it was overnight placed, which is due to the formation of diimine. Also, it was found that Ag$_3$PO$_4$ nanocrystals or H$_2$O$_2$ alone did not produce significant color change (inset of Figure 3). These results confirm that Ag$_3$PO$_4$ nanocrystals behave with peroxidase-like activity toward TMB.

To investigate the effect of pH values of buffer solution on catalytic properties, we performed the catalytic experiments in NaAc buffer with different pH values. Relative activity was analyzed based on the absorption at 652 nm. Fig. 4 shows the relative activity of the Ag$_3$PO$_4$ nanocrystals with reaction time of 30 min at room temperature. It was found that the catalytic activity of Ag$_3$PO$_4$ nanocrystals is significantly affected by pH values. Only very lower catalytic activity was demonstrated when the pH value of buffer exceeds 4.5. We then selected the buffer with pH of 4 for the subsequent study due to the consideration of the possible disability of Ag$_3$PO$_4$ nanocrystals in buffer with strong acidity. With the buffer of pH = 4, a contrast measure was conducted in the absence of Ag$_3$PO$_4$ nanocrystals, which give very low absorbency at 652 nm.

As shown in Fig. 5, the catalytic activity of Ag$_3$PO$_4$ nanocrystals is also H$_2$O$_2$ concentration dependent. With the increasing of H$_2$O$_2$ concentration, the peroxidase-like catalytic activity increases at first. When the concentration of H$_2$O$_2$ reaches about 2.2 mmol/L (that is 7.3 times that of TMB), the catalytic activity of the Ag$_3$PO$_4$ nanocrystals achieves its highest point. However, further increasing the H$_2$O$_2$ concentration causes a lower absorbance at 652 nm, which implies low catalytic activity at higher H$_2$O$_2$ concentration. In fact, many nanoparticle-based enzyme mimics show this kind hump-shaped relationship between H$_2$O$_2$ concentration and the reaction activity including the highly studied enzyme mimic material Fe$_3$O$_4$ [13,44–46]. This phenomenon is also similar to that observed with horseradish peroxidase [13,44]. It is reasonable that the reaction activity increases at first with the increase of H$_2$O$_2$ concentration, since more oxidant is involved in the reaction system. With high concentration of H$_2$O$_2$ in the reaction system, it is usually proposed that the H$_2$O$_2$ moleculars would cap on the surface of catalyst, inhibiting the attachment of substance to the surface of catalyst, and so weakening the catalytic activity. Thus, a hump-shaped relationship is obtained. While, this H$_2$O$_2$ concentration dependent catalytic activity is different from that of CuO [47], Au nanoparticles [38], Ag nanoparticles [48]. In those cases, the reaction acitivity increases monotonously with H$_2$O$_2$ concentration till a saturation state is obtained.

For biomolecular enzymes, the catalytic active center is usually the coordination unsaturated metal sites under the capping of protein networks. For nanoparticles, the surface atoms place in similar situation–coordination unsaturation under the capping of surfactant molecules. Thus, it is possible that they may share some common points in catalytic process, although the catalysis mechanism of inorganic catalysts and enzymes are usually different. At present stage, the Michaelis-Menten model is widely used for the study of nanoparticle-based enzyme mimetics [13,26,49–52]. Therefore, in our study, the Michaelis-Menten

Figure 1. The prepared Ag$_3$PO$_4$ nanoparticles. a) XRD pattern and b) TEM image, the standard pattern of cubic Ag$_3$PO$_4$ with JCPDS No. 06-0505 is also shown for comparison.
doi:10.1371/journal.pone.0109158.g001

Figure 2. The oxidation reaction of TMB.
doi:10.1371/journal.pone.0109158.g002

model was also selected to understand the peroxidase-like catalytic activity of the Ag₃PO₄ nanocrystals.

For further analyzing the catalytic kinetic parameters, the catalytic activity of Ag₃PO₄ nanocrystals was studied by the Michaelis-Menten model with TMB as substrate. The apparent steady-state kinetic parameters for the reaction were determined at 25°C with pH = 4 buffer. Fig. 6a shows the TMB concentration dependent catalytic activity. The absorbance increases with the increasing of TMB concentration, especially at higher TMB concentration range. Absorbance data were then back-calculated to concentrations by the Beer-Lambert Law using a molar absorption coefficient of 39000 $M^{-1}cm^{-1}$ for TMB-derived oxidation product [53].
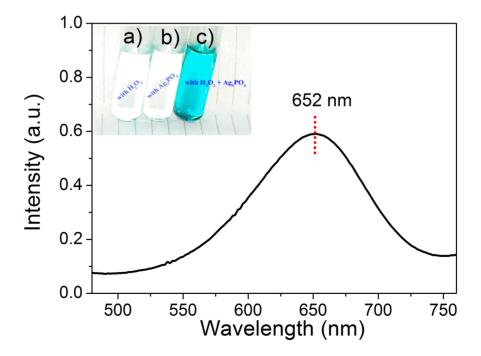
Kinetic parameters were then calculated based on the Michaelis–Menten equation, which

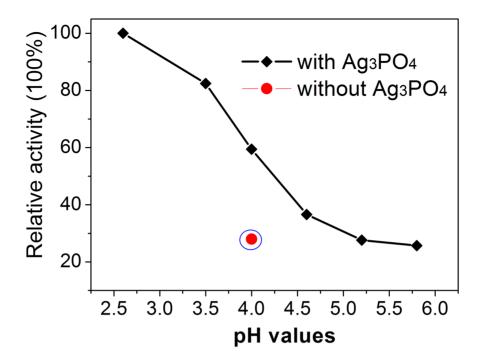$$V_o = \frac{V_{max}[S]}{[S] + K_m} \qquad (1)$$

describes the relationship between the rate of substrate conversion by an enzyme catalyst and the concentration of the substrate. In this equation, V_o is the conversion rate, V_{max} is the maximum conversion rate, $[S]$ is the substrate concentration, and K_m is the Michaelis constant which denotes the affinity of the enzyme. According to (1), a corresponding plot of $1/V_o \sim 1/[S]$ is shown in

Fig. 6b, which reveals that the reaction catalyzed by Ag₃PO₄ nanocrystals follows Michaelis-Menten kinetics in a certain range of substrate concentrations.

The corresponding values of K_m and V_{max} calculated from double reciprocal plots with TMB substrate are 0.327 mM and 2.01×10^{-5} mM s^{-1} (Fig. 6b). By comparing the apparent kinetic parameters, the K_m value of Ag₃PO₄ nanocrystals with TMB substrate is lower than that of reported horserahish peroxidase (HRP, 0.434) tested in buffer solution with pH 3.5 at 40°C [13], suggesting that Ag₃PO₄ nanocrystals have a higher affinity for TMB than HRP. The V_{max} value is similar to that of typical nanomaterial-based enzyme mimetics, Fe₃O₄ nanoparticles. The values of K_m and V_{max} calculated with H₂O₂ substrate are 0.216 mM and 1.27×10^{-5} mM s^{-1} (inset of Fig. 5). The K_m value obtained here with H₂O₂ substrate is lower than that of Fe₃O₄ nanoparticles and HRP [13,19] reported under similar test conditions (buffer solution with pH 3.6–4.6, TMB concentration of 0.2–0.8 mM, temperature of 25°C), suggesting that the Ag₃PO₄ nanocrystals exhibit strong affinity towards TMB and H₂O₂. The strong affinity would be a reason for the excellent peroxidase-like activity.

Fig. 7 shows the time-dependent catalytic activity of four similar reaction systems with different amounts of Ag₃PO₄ nanocrystals. The absorbance of the Ag₃PO₄ catalyzed system is much higher than the one without Ag₃PO₄ catalyst. Among the three Ag₃PO₄

Figure 3. UV-vis spectrum of the reaction system with H₂O₂ + Ag₃PO₄ nanocrystals. The inset shows images of oxidation color reaction of TMB in NaAc buffer with a) H₂O₂, b) Ag₃PO₄ nanocrystals and c) H₂O₂ + Ag₃PO₄ nanocrystals. Reaction conditions: 0.3 mM of TMB, 2 mg/mL of Ag₃PO₄ (if with), 3.6 mM of H₂O₂ (if with) in 5 mL of NaAc buffer with pH 4.0. The reaction proceeded at 25°C with time of 30 min.
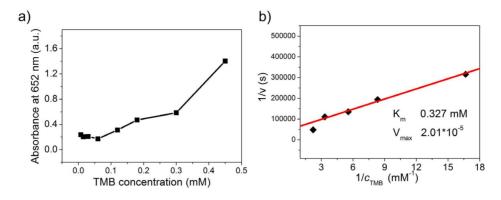doi:10.1371/journal.pone.0109158.g003

Figure 4. pH value-dependent peroxidase-like catalytic activity of Ag$_3$PO$_4$ nanocrystals. Reaction conditions: 0.3 mM of TMB, 2 mg/mL of Ag$_3$PO$_4$, 3.6 mM of H$_2$O$_2$ in 5 mL of NaAc buffer with different pH values. The reaction proceeded at 25°C with time of 30 min.
doi:10.1371/journal.pone.0109158.g004

catalyzed systems, the more catalyst is involved, the higher absorbency is shown. Control experiment to examine the time-dependent absorption spectrum of Ag$_3$PO$_4$ nanocrystals dispersed in buffer solution (pH = 4) at different concentrations (1, 2, 4 mg/mL) gives no obvious change of absorbency with time, indicating

that the increasing absorbency in reaction system is related to the oxidation of TMB, but not originated from the increased concentration of Ag$_3$PO$_4$ nanocrystals (Fig. 7c). These results show that higher reaction rates are obtained with high concentration of Ag$_3$PO$_4$ catalyst. With 4 mg/mL of Ag$_3$PO$_4$ nanocrys-

Figure 5. H$_2$O$_2$ concentration dependent peroxidase-like catalytic activity of Ag$_3$PO$_4$ nanocrystals. Reaction conditions: 0.3 mM of TMB, 2 mg/mL of Ag$_3$PO$_4$ in 5 mL of NaAc buffer with pH 4.0. The concentration of H$_2$O$_2$ varies in the range of 0.36–7.2 mM. The reaction proceeded at 25°C with time of 30 min.
doi:10.1371/journal.pone.0109158.g005

Figure 6. Steady-state kinetic assay of the Ag$_3$PO$_4$ nanocrystals. a) The concentration of H$_2$O$_2$ was 5 mM and the TMB concentration was varied. b) Double reciprocal plots of $1/V \sim 1/C_{TMB}$. Reaction conditions: 2 mg/mL of Ag$_3$PO$_4$ in 5 mL of NaAc buffer with pH 4.0 at 25°C.
doi:10.1371/journal.pone.0109158.g006

tals, it seems that the reaction arrives equilibrium at about 50 minutes. The influence of temperature (10°C, 25°C, 35°C) on the peroxidase-like catalytic activity is also investigated with 20 mg of Ag$_3$PO$_4$ nanocrystals. As shown in Fig. 7b, the Ag$_3$PO$_4$ nanocrystals show the higher peroxidase-like catalytic activity at temperature of 25°C, although in the initial 15 min, the system has a relatively higher reaction rate at 35°C. The temperature dependent catalytic activity is similar to that of natural enzyme or Fe$_3$O$_4$ nanoparticles, which have a preferred temperature.

The use of Ag$_3$PO$_4$ nanocrystals as catalysts for electron-transfer reactions has been rarely investigated, and the in-depth catalytic mechanism is also not clear at present stage. It is proposed Ag$_3$PO$_4$ nanocrystals plays a role of transferring electrons to hydrogen peroxide, causing them to decompose. It is assumed that the oxygen-oxygen bond of H$_2$O$_2$ will rapidly broken by the catalytic action of Ag$_3$PO$_4$ nanocrystals to give OH radicals. The OH radicals stabilize at the surface of the Ag$_3$PO$_4$ nanocrystals, and react with TMB.

In summary, colloidal Ag$_3$PO$_4$ nanocrystals with smaller size were prepared. The peroxides-like catalytic activity of these Ag$_3$PO$_4$ nanocrystals were systematically investigated. The results show that they have a higher activity at acid environment. The catalytic activity was also dependent on H$_2$O$_2$ concentration, temperature, and catalsy amount. Kinetic analysis indicates that the catalysis reaction is in accord with typical Michaelis-Menten kinetics. The apparent kinetic parameters suggest the higher affinity of Ag$_3$PO$_4$ nanocrystals than that of horserahish peroxidase. Our research gives new content to well-known Ag$_3$PO$_4$ material and provides a new nanomaterial-based peroxide enzyme

mimics, which would found applications in medical diagnostics and biochemistry.

Materials and Methods

Synthesis of Ag$_3$PO$_4$ nanocrystals: Ag$_3$PO$_4$ nanocrystals were synthesized with reported methods with minor adjustments [6]. In brief, 8.5 g of AgNO$_3$ and 32 mL of oleylamine were dispersed in 150 mL of toluene and stirred for about 2 h at room temperature. After AgNO$_3$ was fully dissolved, an ethanol solution containing 50 mL of ethanol, 2 mL of H$_2$O, 2.84 mL of H$_3$PO$_4$ was added into the above solution. The solution tuned into yellow colloid quickly. After reaction for 30 mins at room temperature, Ag$_3$PO$_4$ nanocrystals were precipitated by adding ethanol, and washed several times with toluene and ethanol. The dark-yellow precipitate was dried in an oven.

Characterization of Ag$_3$PO$_4$ nanocrystals: The phase structure of the as-synthesized products were characterized using X-ray diffraction (XRD, Bruker D8 ADVANCE) with Cu-Kα radiation ($\lambda = 1.5406$ Å) at a scanning rate of 6° min^{-1}. The morphology and size of the products were examined by a transmission electron microscope (TEM, JEOL JEM-2100) with an accelerating voltage of 200 kV. The Ag$_3$PO$_4$ product dispersed in ethanol was dropped onto a holey copper grid covered with an amorphous carbon film for the TEM examination.

Surface modification for Ag$_3$PO$_4$ nanocrystals: Before property investigation, the obtained Ag$_3$PO$_4$ nanocrystals were firstly treated through usual ligand exchange route [54] to transfer it to being hydrophilic state. Briefly, about 50 mg of Ag$_3$PO$_4$ nanocrystals were dispersed into the mixture of hexane (35 mL),

Figure 7. Time-dependent catalytic activity with a) different amounts of Ag$_3$PO$_4$ nanocrystals at 25°C and b) at different temperature with 4 mg/mL of Ag$_3$PO$_4$ nanocrystals. Reaction conditions: 0.3 mM of TMB, 0–4 mg/mL of Ag$_3$PO$_4$, 3.6 mM of H$_2$O$_2$ in 5 mL of NaAc buffer with pH of 4. c) Control experiment to show the time-dependent absorption spectra of Ag$_3$PO$_4$ nanocrystals dispersed in buffer solution (pH = 4) at different concentrations (1, 2, 4 mg/mL).
doi:10.1371/journal.pone.0109158.g007

distilled water (15 mL), and ethanol (30 mL) through magnetic stirring. Then, 6-amino caproic acid (0.13 g) and equivalent molar NH$_3$·H$_2$O in 5 mL of distilled water was added into the above system. After that, the mixture was heated to 70°C and kept at that temperature for 4 h. The nanocrystals were then collected by centrifugation and washed with water. Through this process, the hydrophobic Ag$_3$PO$_4$ nanocrystals were transformed into hydrophilic state, which can be dispersed in water.

Peroxidase-like catalytic activity of Ag$_3$PO$_4$ nanocrystals: The peroxidase-like activity of freshly treated Ag$_3$PO$_4$ nanocrystals was determined by measuring the formation of a blue charge-transfer complex of diamine from TMB at 652 nm ($\varepsilon = 39000$ M^{-1} cm^{-1}). The TMB oxidation activity measurement, unless otherwise specified, was conducted in sodium acetate buffer (pH 4.0) in the presence of Ag$_3$PO$_4$ nanocrystals (2 mg mL^{-1}) with 0.3 mM of TMB and 3.6 mM of H$_2$O$_2$. The reaction proceeded at 25°C with time of 30 min.

pH Measurements: The activity of the Ag$_3$PO$_4$ nanocrystals at different pH values was performed using the same conditions as above, except different buffer compositions (with different concentration ratios of HAc to NaAc) for different pH values were employed. The reaction was carried out with 2 mg mL^{-1} of Ag$_3$PO$_4$ nanocrystals to which TMB (0.3 mM) and H$_2$O$_2$ (3.6 mM) were added. The pH of the different buffers was adjusted by using a pH meter.

Determination of kinetic parameters: The steady-state kinetics were performed by varying one of the concentrations of Ag$_3$PO$_4$ nanocrystals (0–4 mg mL^{-1}), H$_2$O$_2$ (0.35–7 mM), or TMB (0–0.45 mM) at a time. The reaction was carried out in acetate buffer (pH 4.0) for 30 min and monitored by measuring the absorbency at 652 nm. The kinetic curves were adjusted according to the Michaelis-Menten model.

Author Contributions

Conceived and designed the experiments: YJL. Performed the experiments: YJL GXZ JY. Analyzed the data: AHY XPS. Contributed reagents/materials/analysis tools: GXZ. Contributed to the writing of the manuscript: YJL.

References

1. Katsumata H, Taniguchia M, Kanecoa S, Suzuki T (2013) Photocatalytic Degradation of Bisphenol A by Ag$_3$PO$_4$ under Visible Light. Catal Commun 34: 30–34.
2. Umezawa N, Shuxin O, Ye J (2011) Theoretical Study of High Photocatalytic Performance of Ag$_3$PO$_4$. Phys Rev B 83: 035202.
3. Yi Z, Ye J, Kikugawa N, Kako T, Ouyang S, et al. (2010) An Orthophosphate Semiconductor with Photooxidation Properties under Visible-light Irradiation. Nat Mater 9: 559–564.
4. Bi Y, Ouyang S, Umezawa N, Cao J, Ye J (2011) Facet Effect of Single-Crystalline Ag$_3$PO$_4$ Sub-microcrystals on Photocatalytic Properties. J Am Chem Soc 133: 6490–6492.
5. Bi Y, Hu H, Ouyang S, Lu G, Cao J, et al. (2012) Photocatalytic and Photoelectric Properties of Cubic Ag$_3$PO$_4$ Sub-microcrystals with Sharp Corners and Edges. Chem Commun 48: 3748–3750.
6. Dinh CT, Nguyen TD, Kleitz F, Do TO (2011) Large-scale Synthesis of Uniform Silver Orthophosphate Colloidal Nanocrystals Exhibiting high Visible Light Photocatalytic Activity. Chem Commun 47: 7797–7799.
7. Liang Q-H, Ma W-J, Shi Y, Li Z, Yang X-M (2012) Hierarchical Ag$_3$PO$_4$ Porous Microcubes with Enhanced Photocatalytic Properties Synthesized with the Assistance of Trisodium Citrate. CrystEngComm 14: 2966–2973.
8. Li G-P, Mao L-Q (2012) Magnetically Separable Fe$_3$O$_4$-Ag$_3$PO$_4$ Sub-micrometre Composite: Facile Synthesis, High Visible Light-driven Photocatalytic Efficiency, and Good Recyclability. RSC Adv 2: 5108–5111.
9. Liu L, Liu J-C, Sun DD (2012) Graphene Oxide Enwrapped Ag$_3$PO$_4$ Composite: Towards a Highly Efficient and Stable Visible-Light-Induced Photocatalyst for Water Purification. Catal Sci & Techn 2: 2525–2532.
10. Zhang H-C, Huang H, Ming H, Li H-T, Zhang L-L, et al. (2012) Carbon Quantum dots/Ag$_3$PO$_4$ Complex Photocatalysts with Enhanced Photocatalytic Activity and Stability under Visible Light. J Mater Chem 22: 10501–10506.
11. Zhang L-L, Zhang H-C, Huang H, Liu Y, Kang Z-H (2012) Ag$_3$PO$_4$/SnO$_2$ Semiconductor Nanocomposites with Enhanced Photocatalytic Activity and Stability. New J Chem 36: 1541–1544.
12. Bi Y-P, Ouyang S-X, Cao J-Y, Ye J-H (2011) Facile Synthesis of Rhombic Dodecahedral AgX/Ag$_3$PO$_4$ (X = Cl, Br, I) Heterocrystals with Enhanced Photocatalytic Properties and Stabilities. Phys Chem Chem Phys 13: 10071–10075.
13. Gao L-Z, Zhuang J, Nie L, Zhang J-B, Zhang Y, et al. (2007) Intrinsic Peroxidase-like Activity of Ferromagnetic Nanoparticles. Nat Nanotechnol 2: 577–583.
14. Wei H, Wang E (2008) Fe$_3$O$_4$ Magnetic Nanoparticles as Peroxidase Mimetics and their Applications in H$_2$O$_2$ and Glucose Detection. Anal Chem 80: 2250–2254.
15. Yu F, Huang Y, Cole AJ, Yang VC (2009) The Artificial Peroxidase Activity of Magnetic Iron Oxide Nanoparticles and its Application to Glucose Detection. Biomaterials 30: 4716–4722.
16. Wang N, Zhu L, Wang M, Wang D, Tang H (2010) Sono-assisted Preparation of Highly-efficient Peroxidase-like Fe$_3$O$_4$ Magnetic Nanoparticles for Catalytic Removal of Organic Pollutants with H$_2$O$_2$. Ultrason Sonochem 17: 526–533.
17. Zuo X, Peng C, Huang Q, Song S, Wang L, et al. (2009) Design of a Carbon nanotube/Magnetic Nanoparticle-based Peroxidase-like Nanocomplex and its Application for Highly Efficient Catalytic Oxidation of Phenols. Nano Res 2: 617–623.
18. He S, Shi W, Zhang X, Li J, Huang Y (2010) β-Cyclodextrins-based Inclusion Complexes of CoFe$_2$O$_4$ Magnetic Nanoparticles as Catalyst for the Luminol Chemiluminescence System and their Applications in Hydrogen Peroxide Detection. Talanta 82: 377–383.
19. Zhang XQ, Gong SW, Zhang Y, Yang T, Wang CY, et al. (2010) Prussian Blue Modified Iron Oxide Magnetic Nanoparticles and Their High Peroxidase-like Activity. J Mater Chem 20: 5110–5116.
20. Liu S, Lu F, Xing R, Zhu JJ (2011) Structural Effects of Fe$_3$O$_4$ Nanocrystals on Peroxidase-Like Activity. Chem Eur J 17: 620–625.
21. Niu H, Zhang D, Zhang S, Zhang X, Meng Z, et al. (2011) Humic Acid Coated Fe$_3$O$_4$ Magnetic Nanoparticles as Highly Efficient Fenton-like Catalyst for Complete Mineralization of Sulfathiazole. J Hazard Mater 190: 559–565.
22. Park KS, Kim MI, Cho DY, Park HG (2011) Label-Free Colorimetric Detection of Nucleic Acids Based on Target-Induced Shielding against the Peroxidase-Mimicking Activity of Magnetic Nanoparticles. Small 7: 1521–1525.
23. Shi W, Zhang X, He S, Huang Y (2011) CoFe$_2$O$_4$ Magnetic Nanoparticles as a Peroxidase Mimic Mediated Chemiluminescence for Hydrogen Peroxide and Glucose. Chem Commun 47: 10785–10787.
24. Korsvik C, Patil S, Seal S, Self WT (2007) Superoxide Dismutase Mimetic Properties Exhibited by Vacancy Engineered Ceria Nanoparticles. Chem Commun 1056–1058.
25. Heckert EG, Karakoti AS, Seal S, Self WT (2008) The Role of Cerium Redox State in the SOD Mimetic Activity of Nanoceria. Biomaterials 29: 2705–2709.
26. Asati A, Santra S, Kaittanis C, Nath S, Perez JM (2009) Oxidase-Like Activity of Polymer-Coated Cerium Oxide Nanoparticles. Angew Chem Int Ed 48: 2308–2312.
27. Pirmohamed T, Dowding JM, Singh S, Wasserman B, Heckert E, et al. (2010) Nanoceria Exhibit Redox State-dependent Catalase Mimetic Activity. Chem Commun 46: 2736–2738.
28. Andre R, Natalio F, Humanes M, Leppin J, Heinze K, et al. (2011) V$_2$O$_5$ Nanowires with an Intrinsic Peroxidase-Like Activity. Adv Funct Mater 21: 501–509.
29. Song Y, Qu K, Zhao C, Ren J, Qu X (2010) Graphene Oxide: Intrinsic Peroxidase Catalytic Activity and its Application to Glucose Detection. Adv Mater 22: 2206–2210.
30. Song Y, Wang X, Zhao C, Qu K, Ren J, et al. (2010) Label-Free Colorimetric Detection of Single Nucleotide Polymorphism by Using Single-Walled Carbon Nanotube Intrinsic Peroxidase-Like Activity. Chem Eur J 16: 3617–3621.
31. Qu F, Li T, Yang M (2011) Colorimetric Platform for Visual Detection of Cancer Biomarker Based on Intrinsic Peroxidase Activity of Graphene Oxide. Biosens Bioelectron 26: 3927–3931.
32. Cui R, Han Z, Zhu JJ (2011) Helical Carbon Nanotubes: Intrinsic Peroxidase Catalytic Activity and Its Application for Biocatalysis and Biosensing. Chem Eur J 17: 9377–9384.
33. Song Y, Chen Y, Feng L, Qu X (2011) Selective and Quantitative Cancer Cell Detection Using Target-directed Functionalized Graphene and its Synergetic Peroxidase-like Activity. Chem Commun 47: 4436–4438.
34. Shi W, Wang Q, Long Y, Cheng Z, Chen S, et al. (2011) Carbon Nanodots as Peroxidase Mimetics and their Applications to Glucose Detection. Chem Commun 47: 6695–6697.
35. Wang X, Qu K, Xu B, Ren J, Qu X (2011) Multicolor Luminescent Carbon Nanoparticles: Synthesis, Supramolecular Assembly with Porphyrin, Intrinsic Peroxidase-like Catalytic Activity and Applications. Nano Res 4: 908–920.
36. Song Y, Wei W, Qu X (2011) Colorimetric Biosensing Using Smart Materials. Adv Mater 23: 4215–4236.

37. He W, Wu X, Liu J, Hu X, Zhang K, et al. (2010) Design of AgM Bimetallic Alloy Nanostructures (M = Au, Pd, Pt) with Tunable Morphology and Peroxidase-like Activity. Chem Mater 22: 2988–2994.

38. Jv Y, Li B, Cao R (2010) Positively-charged Gold Nanoparticles as Peroxidiase Mimic and their Application in Hydrogen Peroxide and Glucose Detection. Chem Commun 46: 8017–8019.

39. Fan J, Yin JJ, Ning B, Wu X, Hu Y, et al. (2011) Direct Evidence for Catalase and Peroxidase Activities of Ferritin–platinum nanoparticles. Biomaterials 32: 1611–1618.

40. He W, Liu Y, Yuan J, Yin JJ, Wu X, et al. (2011) Au@ Pt nanostructures as Oxidase and Peroxidase Mimetics for Use in Immunoassays. Biomaterials 32: 1139–1147.

41. Liu J, Hu X, Hou S, Wen T, Liu W, et al. (2011) Screening of Inhibitors for Oxidase Mimics of Au@ Pt Nanorods by Catalytic Oxidation of OPD. Chem Commun 47: 10981–10983.

42. Wang X-X, Wu Q, Shan Z, Huang QM (2011) BSA-stabilized Au Clusters as Peroxidase Mimetics for use in Xanthine Detection. Biosens Bioelectron 26: 3614–3619.

43. Josephy PD, Eling TE, Mason RP (1982) The Horseradish Peroxidase-catalyzed Oxidation of 3,5,3′,5′-Tetramethylbenzidine: Free Radical and Charge-transfer Complex Intermediates. J Biol Chem 257: 3669–3675.

44. Tian J-Q, Liu S, Luo YL, Sun X-P (2012) Glucose Oxidation Using Au-containing Bimetallic and Trimetallic Nanoparticles. Catal Sci Technol 2: 432–436.

45. Ma M, Zhang Y, Gu N (2011) Peroxidase-like Catalytic Activity of Cubic Pt Nanocrystals. Colloids and Surfaces A: Physicochem. Eng. Aspects 373: 6–10.

46. Dong Y-L, Zhang H-G, Rahman ZU, Su L, Chen XJ, et al. (2012) Graphene oxide-Fe$_3$O$_4$ Magnetic Nanocomposites with Peroxidase-like Activity for Colorimetric Detection of Glucose. Nanoscale 4: 3969–3976.

47. Chen W, Chen J, Feng YB, Hong L, Chen QY, et al. (2012) Peroxidase-like Activity of Water-soluble cupric Oxide Nanoparticles and its Analytical Application for Detection of Hydrogen Peroxide and Glucose. Analyst 137: 1706–1712.

48. Jiang H, Chen Z, Cao H, Huang Y (2012) Peroxidase-like Activity of Chitosan Stabilized Silver Nanoparticles for Visual and Colorimetric Detection of Glucose. Analyst 137: 5560–5564.

49. Liu J-B, Hua X, Hou S, Wen T, Liu W-Q, et al. (2012) Au@Pt Core/shell Nanorods with Peroxidase- and Ascorbate Oxidase-like Activities for Improved Detection of Glucose. Sensors and Actuators B166–167: 708–714.

50. Dutta AK, Maji SK, Srivastava DN, Mondal A, Biswas P, et al. (2012) Synthesis of FeS and FeSe Nanoparticles from a Single Source Precursor: A Study of Their Photocatalytic Activity, Peroxidase-Like Behavior, and Electrochemical Sensing of H$_2$O$_2$. ACS Appl. Mater. Interfaces 4: 1919–1927.

51. Sun X-L, Guo S-J, Chung C-S, Zhu W-L, Sun S-H (2013) A Sensitive H$_2$O$_2$ Assay Based on Dumbbell-like PtPd-Fe$_3$O$_4$ Nanoparticles. Adv Mater 25: 132–136.

52. Wang Q, Liu S-W, Sun H-Y, Lu Q-F (2014) Synthesis and Intrinsic Peroxidase-Like Activity of Sisal-Like Cobalt Oxide Architectures. Ind. Eng. Chem. Res. 53: 7917–7922.

53. Karaseva EI, Losev YP, Metelitsa DI (2002) Peroxidase-catalyzed Oxidation of 3, 3″, 5, 5″-Tetramethylbenzidine in the Presence of 2, 4-Dinitrosoresorcinol and Polydisulfide Derivatives of Resorcinol and 2, 4-Dinitrosoresorcinol. Russ J Bioorg Chem 28: 128–135.

54. Tian Q-W, Jiang F-R, Zou R-J, Liu Q, Chen Z-G, et al. (2011) Hydrophilic Cu$_9$S$_5$ Nanocrystals: A Photothermal Agent with a 25.7% Heat Conversion Efficiency for Photothermal Ablation of Cancer Cells in Vivo. ACS Nano 5: 9761–9771.